

Article pubs.acs.org/iournal/abseba

Piezoelectric Heterogeneity in Collagen Type I Fibrils Quantitatively Characterized by Piezoresponse Force Microscopy

Jinha Kwon and Hanna Cho*



Cite This: ACS Biomater. Sci. Eng. 2020, 6, 6680-6689



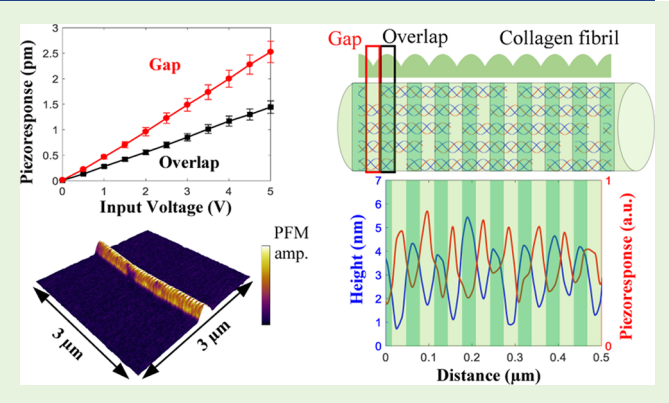
ACCESS I

III Metrics & More

Article Recommendations

Supporting Information

ABSTRACT: Piezoelectricity of Type I collagen can provide the stress-generated potential that is considered to be one of the candidate mechanisms to explain bone's adaptation to loading. However, it is still challenging to quantify piezoelectricity because of its heterogeneity and small magnitude. In this study, resonanceenhanced piezoresponse force microscopy (PFM) was utilized to amplify a weak piezoresponse of a single collagen fibril with a carefully calibrated cantilever. The quantitative PFM, combined with a dual-frequency resonance-tracking method, successfully identified the anisotropic and heterogenous nature of the piezoelectric properties in the collagen fibril. The profile of shear piezoelectric coefficient (d_{15}) was obtained to be periodic along the collagen fibril, with a larger value in the gap zone (0.51 pm/V) compared to the value in the overlap zone (0.29 pm/V).



Interestingly, this piezoelectric profile corresponds to the periodic profile of mechanical stiffness in a mineralized collagen fibril having a higher stiffness in the gap zone. Considering that apatite crystals are nucleated at the gap zone and subsequently grown along the collagen fibril, the heterogeneous and anisotropic nature of piezoelectric properties highlights the physiological importance of the collagen piezoelectricity in bone mineralization.

KEYWORDS: type I collagen, collagen fibril, piezoelectricity, piezoresponse force microscopy, atomic force microscopy, dual-frequency resonance-tracking piezoresponse force microscopy

1. INTRODUCTION

Piezoelectricity is the electrical potential induced by mechanical stress in crystalline or structured materials. In the 1960s, the experimental demonstration of the piezoelectric effect in bone had drawn a substantial interest among researchers in elucidating the bone's ability to adapt itself to mechanical stresses, known as "Wolff's Law". 1-6 Subsequent studies confirmed that the bone piezoelectricity is mainly attributed to tropocollagen because of its specific arrangement of collagen molecules (i.e., polypeptide chains) possessing a dipole moment characterized by a N-terminal (NH3+) and C-terminal (COO⁻).⁷⁻⁹ A tropocollagen molecule has a non-centrosymmetric structure ascribed to its triple helix configuration with a hexagonal assembly of collagen molecules in its cross-section, which results in the piezoelectric effect. 10 The tropocollagen molecules assemble again in a staggered manner to build a collagen fibril, a fundamental building base of bone, that exhibits a periodic pattern of repeated gap and overlap regions with a signature D-periodic distance of ~67 nm. 11-16 As a result, a collagen fibril has anisotropic piezoelectricity that is largest on the fibril surface when the bone is loaded in the longitudinal direction.1,17

A bone remodels its structure and composition by replacing its old part with new one by responding to various types of external loading conditions. 12 This newly formed bone mainly consists of soft organic matrix (i.e., Type I collagen) that is subsequently mineralized to enhance the elasticity and hardness of the bone tissue. 18 Although this bone mineralization process is essential to determine bone's material integrity, the underlying driving force and detailed mechanism have not been fully clarified. Considering that the collagen piezoelectricity can generate an electrical potential on the collagen surface in response to the various types of mechanical stress, piezoelectricity is a highly appealing mechanism to explain bone's selective adaptation to varied physiological loading environments. In addition, it was recently reported that a mineralized collagen fibril shows heterogeneous nature in mechanical properties along the collagen fibrillar direction, exhibiting higher

September 3, 2020 Received: Accepted: October 23, 2020 Published: November 10, 2020





Table 1. Piezoelectric Property of Collagen in Published Literature

author	$\begin{array}{c} d_{31} \left(d_{32} \right) \\ \left(\mathrm{pm/V} \right) \end{array}$	d ₃₃ (pm/V)	$d_{14} (-d_{25}) \ (\text{pm/V})$	$d_{15} (d_{24}) (pm/V)$	sample	year	method
Fukada and Yasuda ¹	0.087	0.067	-2.668	1.407	bovine achilles tendon	1964	ballistic galvanometer and mechanical level
	0.013	0.067	-1.901	0.534	horse achilles tendon		
Kalinin et al. ²³	N/A	0.15-0.25	N/A	N/A	single collagen fibril in enamel	2005	VPFM
Majid et al. ⁷	N/A	N/A	N/A	~1	collagen fibril from bovine achilles tendon	2009	LPFM
Denning et al. ²⁸	N/A	N/A	N/A	1.6	collagen membrane	2014	LPFM
Zhou et al. ⁹	N/A	1.10	N/A	N/A	collagen molecule computer model	2016	molecular dynamics simulations
	N/A	2.64	N/A	N/A	collagen microfibril computer model		
Denning et al. ¹⁷	-4.84 ± 2.96	0.89 ± 0.08	-12.00 ± 2.60	6.21 ± 2.93	rat tail tendon	2017	VPFM LPFM

mechanical stiffness in the gap regions.¹⁹ In the mineralization process, it was observed that the minerals infiltrate through the gap regions and spontaneously crystalize, growing along the collagen fibrillar direction.^{20–22} Here, we hypothesize that the collagen piezoelectricity, as one of main contributors, mediates this mechanical heterogeneity of mineralized collagen by providing a heterogeneous template to control the local mineralization along the fibril. In this regard, this work aims to precisely characterize the local piezoelectric property of a collagen fibril.

Piezoresponse force microscopy (PFM) enables characterization of electromechanical properties with a nanometer resolution and has been employed to measure various piezoelectric materials including collagen. 23-27 Table 1 summarizes the piezoelectric property of collagen measured on teeth, tendon, and fibril. 1,7,9,17,23,28 Previous PFM demonstrations indicated that collagen is indeed anisotropically piezoelectric and relatively dominant in the shear piezoelectric direction, but the reported quantitative values vary quite significantly. These inconsistent values of the previous measurements may result from inherent limitations of the conventional PFM technique on quantifying the piezoelectric properties of biomaterials that have high heterogeneous topography and weak piezoelectricity. 29-31 More importantly, recent studies reported that displacements measured by PFM are possibly misinterpreted as piezoelectric response, because there exist alternate origins for the electromechanical displacement such as electrostatic forces. 32-35 Thus, accurate validation of PFM amplitude on collagen with a careful removal of electrostatic contribution is necessary.

In this work, the piezoelectric coefficient of collagen fibrils in air is quantitatively measured by employing resonanceenhanced PFM to amplify the weak piezoresponse of collagen by a quality factor with a careful calibration of cantilever dynamics, while the unwanted electrostatic effect is removed from the measured response. Moreover, the effect of substrate's conductivity on the PFM result was examined. The detailed experimental protocol for quantitative PFM is specified and thoroughly discussed. We also employed dual-frequency resonance-tracking PFM based on a multifrequency atomic force microscopy (AFM) technique to get a piezoelectric profile along a collagen fibril with the topographic crosstalk removed.^{36–39} The quantitative PFM measurements confirm the heterogenous piezoelectric property at the gap and overlap regions along with the anisotropic characteristic without ambiguity.

2. RESULTS AND DISCUSSION

Figure 1 shows the schematic of PFM, based on AFM. A metal-coated AFM cantilever is used to apply an AC voltage to a

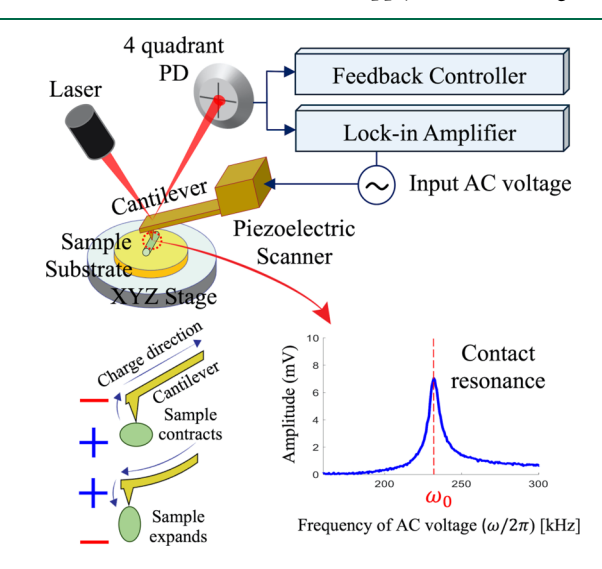


Figure 1. Resonance-enhanced PFM schematic: a metal-coated AFM cantilever scans over a sample surface, and an AC voltage at the contact resonance frequency (ω_0) is applied to the sample surface through the conductive cantilever tip. In response to the electrical stimulus, the sample locally expands or contracts because of the piezoelectric effect, and the local piezoelectric response is amplified and detected by measuring the first harmonic component of the tip deflection.

sample through its conductive tip that is in contact with the sample. In response to the local, nanoscale electrical stimulus at a fixed frequency, the sample produces mechanical strains because of the piezoelectric effect, and the local piezoelectric response is detected by measuring the tip deflection. During PFM scanning, the vertical (flexural) and lateral (torsional) deflection of the cantilever can be separately measured to characterize the direction of sample polarization. 40-42 In vertical PFM, out-ofplane polarization is measured by recording the tip-deflection signal at the modulation frequency. In lateral PFM, the in-plane component of polarization is detected by a lateral motion of the cantilever because of voltage-induced surface shearing. 43-45 In this study, these vertical and lateral PFM techniques were used to characterize the anisotropic piezoelectricity of a collagen fibril using a commercial AFM system (MPF-3D infinity, Asylum Research) and a gold-coated cantilever (0.3 N/m of nominal stiffness, 3XC-GG, OPUS).

In order to determine the direction-dependent piezoelectric coefficient of a collagen fibril, the relationship between the measured (laboratory) and sample coordinate system must be considered. Figure 2 shows the coordinates of the AFM system

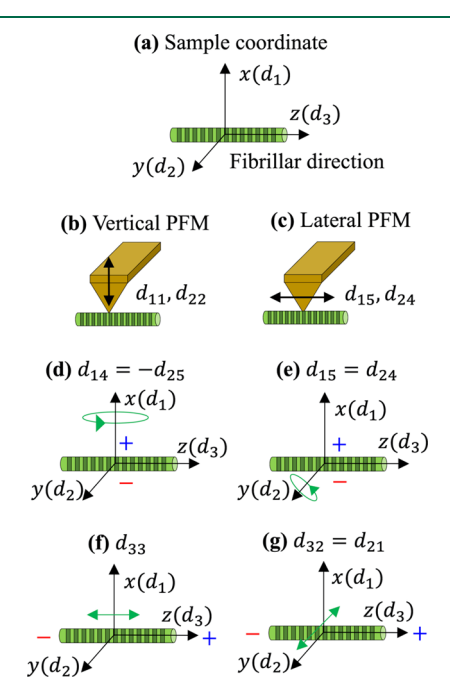


Figure 2. Cantilever set in the *y*-axis to make a perpendicular orientation between the cantilever and collagen fibril. The plus and minus signs denote the applied electric polarity, and the green arrows denote its piezoresponse direction.

and collagen, in which the cantilever body is set in y-axis to make a perpendicular orientation between the cantilever and collagen fibril. The plus and minus signs denote the applied electric polarity, and the green arrows denote its piezoresponse directions. In this measurement setting, $d_{11} = d_{22}$ and $d_{15} = d_{24}$ can be evaluated through vertical and lateral PFM, respectively.

Other piezoelectric tensors $(d_{31}, d_{33}, \text{ and } d_{14})$ cannot be obtained through this measurement configuration because the electric potential cannot be applied along the fibril's longitudinal direction to measure d_{31} and d_{33} ; a collagen fibril was fixed on the substrate resulting in nullification in the d_{14} direction. Regarding the hexagonal/tetragonal symmetry of a collagen fibril, it was assumed that $d_{14} = -d_{25}$, $d_{15} = d_{24}$, and $d_{32} = d_{31}$. Therefore, the piezoelectric tensor can be described by eq 1.

$$d_{ij} = \begin{bmatrix} 0 & 0 & 0 & d_{14} & d_{15} & 0 \\ 0 & 0 & 0 & d_{15} & -d_{14} & 0 \\ d_{31} & d_{31} & d_{33} & 0 & 0 & 0 \end{bmatrix}$$

$$(1)$$

While PFM has been widely applied to characterize various piezoelectric materials, its applications to biomaterials are still challenging because they typically display weak piezoelectricity and are heterogeneous in terms of topography and material. ^{27,48} To amplify the weak piezoelectric signal of collagen, the resonance enhancement technique that employs contact resonance of a cantilever can be utilized. ⁴⁹ Using a harmonic oscillator model, the amplitude and phase responses of resonance-enhanced PFM can be described as ⁵⁰

$$A(\omega) = \frac{\delta}{\sqrt{\left(1 - \left(\frac{\omega}{\omega_0}\right)^2\right)^2 + \left(\frac{\omega}{Q \cdot \omega_0}\right)^2}}$$

$$\tan \phi(\omega) = \frac{\omega/\omega_0}{Q\left(1 - \left(\frac{\omega}{\omega_n}\right)^2\right)}$$
(2)

where δ is the input piezoelectric displacement at the tip, ω is the frequency of the applied AC voltage, ω_0 is the contact resonance frequency, and Q is the quality factor, respectively. When the frequency of the applied voltage is chosen to be the same as the contact resonance frequency (i.e., $\omega=\omega_0$), the mechanical strain of a sample δ is amplified by the quality factor Q according to eq 2. The quality factor of an AFM cantilever is typically in the

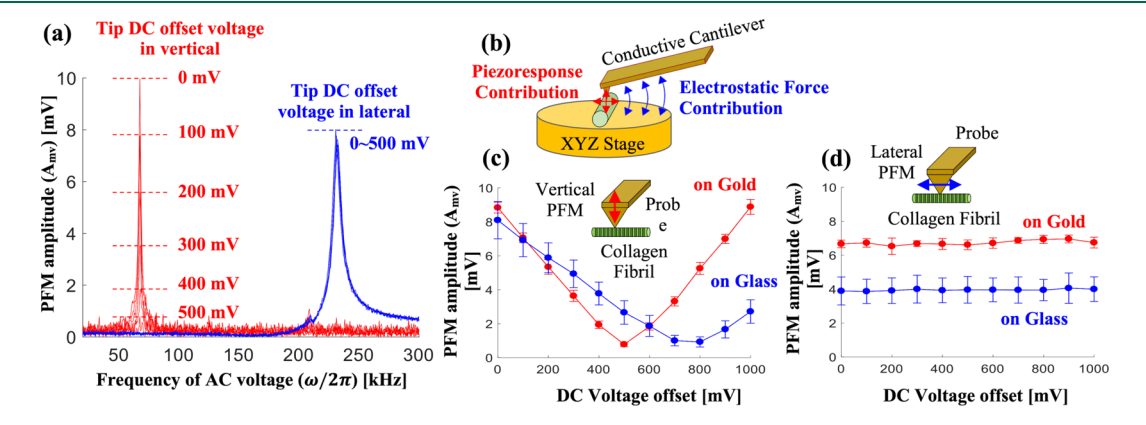


Figure 3. PFM amplitudes measured on the gap region of a collagen fibril in air. (a) Measured amplitudes in the vertical (red) and lateral (blue) direction are plotted as a function of frequency of applied AC voltage ($V_{\rm ac} = 5 \, \rm V$). An DC offset voltage concurrently applied to the sample was varied between 0 and 1 V by 100 mV, and the results from 0–500 mV are shown in the graph. The contact resonance was clearly measured at 67.5 kHz in the flexural mode and at 231.9 kHz in the torsional mode. The DC voltage changes the resonance amplitude of the flexural mode, whereas the lateral results are not affected by the DC voltage. (b) Schematic of piezoelectric and electrostatic force contributions during PFM measurements. (c) PFM amplitudes at the resonance frequency ($\omega = \omega_{0,\text{flexural}}$) in the vertical direction as a function of DC voltage. When the electrostatic force was eliminated at 500 mV (800 mV) in the measurement on collagen prepared on a gold (glass) surface, no significant PFM amplitude was shown. (d) PFM amplitudes at the resonance frequency ($\omega = \omega_{0,\text{torsional}}$) in the lateral direction as a function of DC voltage. The lateral amplitude was not affected by the electrostatic force, and the collagen on a gold surface exhibited a larger amplitude compared with the collagen on a glass surface.

range of several tens to hundreds and, thus, the small piezoelectric strain δ can be amplified to $A_{\rm resonance} = Q\delta$ through the resonance amplification, where $\omega = \omega_0$. Figure 3a shows the contact resonance response curves in the flexural (vertical) and torsional (lateral) modes. The amplitudes were measured on the gap region of a single collagen fibril, prepared on a gold-coated substrate, in the vertical (red) and lateral (blue) directions, while the drive frequency was swept between 0-300 kHz with an applied AC voltage of $V_{\rm ac}$ = 5 V. The obtained contact resonance curves were fitted to eq 2 using the Levenberg–Marquardt algorithm, 51 and the contact resonance frequency (ω_0) and quality factor (Q) were obtained to be 67.5 kHz and 58 in the vertical response and 232.5 kHz and 40 in the lateral response.

When an electrical potential is applied to the metal-coated cantilever during PFM, there can exist a concurrent electrostatic effect in addition to the piezoelectric effect, as illustrated in Figure 3b. The electrostatic force mainly originates from the interactions between the conductive cantilever body and a substrate. This unwanted electrostatic contribution is amplified together with the piezoelectric response when the resonance-enhanced PFM is employed. Therefore, it is important to quantify and remove the electrostatic contribution from the measured PFM response. For the resonance-enhanced PFM, the electrostatic force contribution in the measured response can be estimated by 32

$$A_{\text{electrostatic}} = \left| k^{-1} \left(\frac{dC}{dZ} \right) V_{\text{ac}} (V_{\text{dc}} - V_{\text{sp}}) \right| \cdot Q \tag{3}$$

where k is the spring constant of a cantilever, V_{ac} is the applied AC voltage, V_{dc} is the applied DC voltage, and V_{sp} is the surface potential. The resulting electrostatic amplitude is inversely proportional to cantilever's spring constant k and proportional to the capacitance derivative dC/dz, $V_{\rm ac}(V_{\rm dc}-V_{\rm sp})$, and Q factor. This implies that the impact of the electrostatic force can be reduced by either (i) using a stiff cantilever (i.e., $k^{-1} \ll 1$) or (ii) applying an external DC voltage $V_{\rm dc}$ to be equal to the surface potential $V_{\rm sp}$ (i.e., $V_{\rm dc} = V_{\rm sp}$). As a biological sample is commonly soft enough to be easily damaged by a stiff cantilever, the second option is more practical to eliminate the electrostatic contribution. As the surface potential of a measured surface is typically unknown, the PFM amplitude was measured with varied DC bias from 0 to 1 V by 100 mV steps to find a compensating DC voltage that is same as the surface potential $V_{\rm sp}$. It is worth noting that kelvin probe force microscopy can be also employed at this step as an alternative method to measure the surface potential. 52 Figure 3c,d shows PFM amplitudes at the contact resonance frequency with respect to the DC voltage offset in the vertical and lateral directions, respectively. The resulting V-shape in the vertical amplitude can be interpreted that the vertical PFM amplitude, greatly affected by the electrostatic force, is nullified at 500 mV, where $V_{\rm dc} = V_{\rm sp}$ (cf. the minimum point of the red curve in Figure 3c). When the electrostatic force contribution was nullified, the vertical PFM amplitude was measured below the system's noise level even with the resonance amplification. This observation verifies that there is no significant piezoresponse of the collagen fibril in the vertical direction $(d_{11}, d_{22} \approx 0)$ as expected in the collagen with hexagonal/tetragonal symmetry. 26 On the other hand, the lateral PFM amplitude was not changed by the DC voltage, indicating that the electrostatic force does not affect the lateral PFM results. This difference between the vertical and lateral PFM is attributed to the derivative capacitance dC/dz term in eq 3. For

vertical PFM, the gaps between the cantilever body and sample is changed during measurement, and thus, the derivative capacitance varies. On the other hand, the gap and derivative capacitance are fairly constant for lateral PFM. Taken together, these results draw a conclusion that the electrostatic force should be carefully eliminated by applying a suitable DC voltage in the vertical PFM, whereas this process is not necessary in the lateral PFM. This conclusion confirms that the variations in the collagen piezoelectricity summarized in Table 1 are not at least caused by an error because of the electrostatic force contribution on the lateral PFM.

The effect of substrate's conductivity on the PFM result was also investigated by repeating the measurement on collagen fibrils prepared on a glass slide, as shown in Figure 3c,d. Each PFM amplitude is illustrated by red lines for the conductive gold substrate and blue lines for the non-conductive glass substrate. In the vertical PFM results, both results showed that there was no piezoelectric response in the vertical direction once the electrostatic force contribution was eliminated, while the nullifying DC voltage was shifted from 500 mV for the conductive substrate to 800 mV for the nonconductive substrate. In lateral PFM, the amplitude on the gold substrate was larger than the amplitude measured on the glass substrate. These results indicate that the nonconductive substrate does not provide a good electrical ground, which reduces the actual electrical field induced across the collagen fibril. Therefore, it is important to prepare a biological sample on a conductive substrate to provide a good ground condition for PFM.

Figure 4 highlights the necessity of using a soft cantilever and a relatively low electrical input, showing a collagen fibril damaged

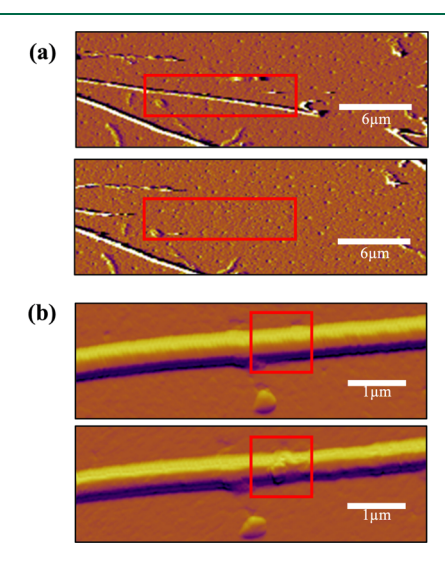
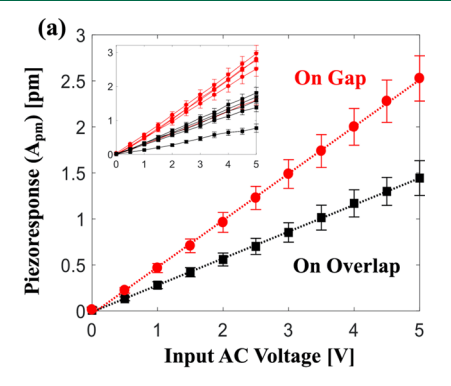


Figure 4. (a) Intact collagen fibril is imaged with a soft cantilever (0.3 N/m) in the upper figure. When a stiff cantilever (2 N/m) is used, the collagen in the red box is damaged and disappears in the lower figure. (b) After a high voltage of 30 V was applied to an intact collagen fibril (upper image), the same area was scanned again to check any damage on the collagen (lower image). It was clearly shown that the collagen fibril was electrically damaged within the marked area.

by a high mechanical or electrical input. In Figure 4a, a collagen fibril was scratched and disappeared after scanning when an AFM cantilever with 2 N/m stiffness was used. Because a contact scanning mode was employed for PFM, a single collagen fibril does not have enough cross-linking, compared to a bundle of collagen fibrils, to sustain a large mechanical input. In addition, a

biological sample is also vulnerable to the high electrical input. As shown in Figure 4b, the intact collagen fibril on a glass slide was permanently damaged by an AC electrical input of 30 V. In our experimental setting, the extent of electrical damage on a fibril was also affected by an electrical ground condition. For instance, it was observed that a collagen fibril prepared on a conductive substrate was easily damaged by an AC electrical input of 10 V. This is the reason behind why the mechanism of resonance amplification is beneficial for such a weak biomaterial sample.

Figure 5a shows the lateral piezoresponse quantitatively measured on a single collagen fibril on the gap (red) and overlap



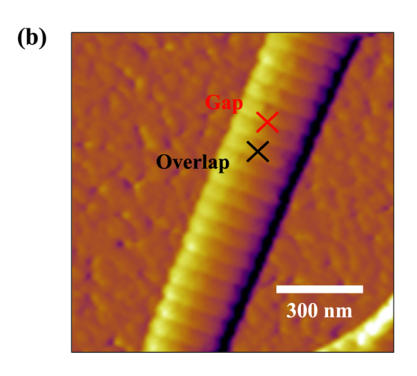


Figure 5. Piezoresponse of Type I collagen fibril in the lateral direction. (a) Average of piezoresponse amplitudes as a function of input AC voltage, measured on five collagen fibrils. The amplitudes of each collagen fibril are shown in the inset with red lines measured on the gap region and black lines measured on the overlap region. (b) AFM deflection map on a collagen fibril. The PFM was conducted at the marked point at the gap (red) and overlap (black) regions.

(black) regions, following the careful calibration process, as described in Section 4. The PFM was conducted at room temperature (22 °C) and 40% relative humidity. The probe was carefully positioned at the gap and overlap region, as marked in Figure 5b, during the measurement. Five individual fibrils on a gold-coated glass substrate were measured, and the measurement was performed 10 times on each collagen fibril at each input AC voltage. In total, 550 data points were obtained on each fibril. The inset of Figure 5a shows the piezoresponse of the five individual collagen fibrils. Although there are small variations of piezoresponse amplitude from fibril to fibril, the piezoresponse of each fibril was repeatable. The average piezoresponse with respect to the applied voltage shows a linear relationship, and the gap region exhibits a higher piezoresponse. The piezoelectric coefficient is obtained from the slope to be 0.51 ± 0.08 pm/V for the gap zone, which is almost twofold higher than the piezoelectric coefficient of 0.29 ± 0.05 pm/V

estimated on the overlap region. This quantitative discrepancy verifies the heterogeneous nature of the piezoelectric property along the collagen fibril. Note that the piezoelectric coefficient of d_{15} was reported at the range of 0.5–1.5 pm/V in the previous studies. 1,7,9,17,23,28

The PFM map on a collagen fibril, as shown in Figure 6, visualizes how the piezoresponse varies within a collagen fibril.

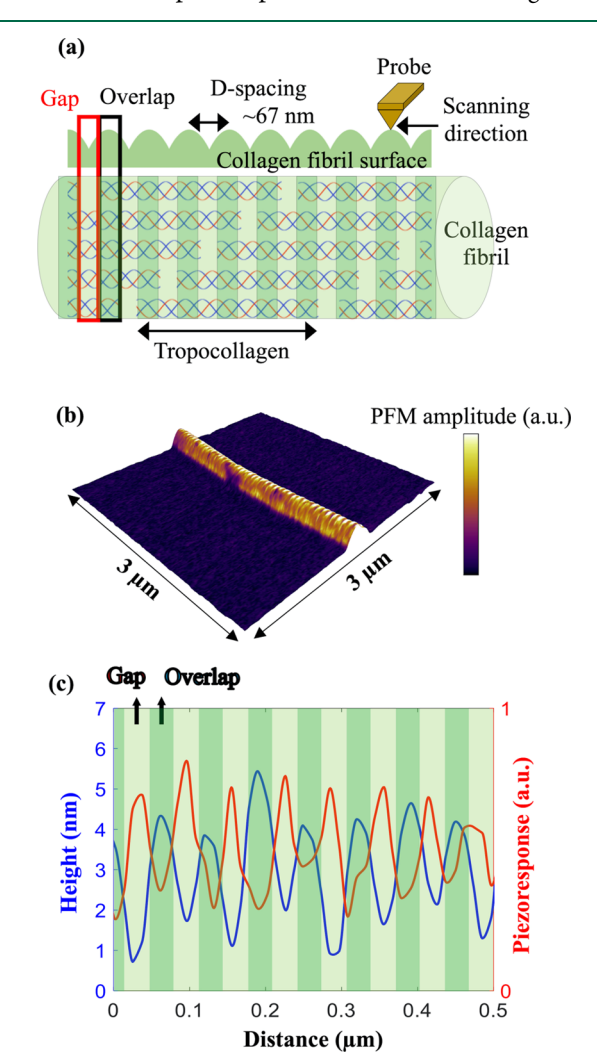


Figure 6. (a) Schematic of a collagen fibril and AFM scanning direction. (b) PFM amplitude overlaid on topography of a single collagen fibril, measured by DART-PFM; (c) height and PFM amplitude profile along the crest of the collagen fibril clearly shows the piezoelectric heterogeneity inversely correlated to the topographic pattern.

Figure 6a illustrates a schematic of a collagen fibril, describing the gap and overlap region and PFM scanning direction on the fibril. Figure 6b represents the PFM amplitude color map overlaid on the topography of a single collagen fibril to clearly reveal its heterogeneity. Obtaining the PFM map, not point measurement, should be considered carefully because of the crosstalk between surface topography and piezoelectric responses. During PFM mapping, the changes in the topography and mechanical properties shift the contact resonance frequency, and this frequency change affects the PFM amplitude as well. To avoid this cross-talk effect, we employed dual AC resonance tracking PFM (DART-PFM). In DART-PFM, the change of the contact resonance frequency can be tracked and compensated, so that the crosstalk between PFM

amplitudes and topographic/material property change is minimized. The mechanism of DART-PFM and its result compared to a common PFM result are shown in the Supporting Information section. It is worth noting that sequential excitation piezoresponse force microscopy (SE-PFM) can be also employed as an alternative method to eliminate the crosstalk. 55-57 The surface topographic and piezoelectric profiles along the crest of the fibril are plotted in Figure 6c. The signature D-periodic pattern was clearly observed in the surface profile (blue), and the PFM amplitude (red) was also repeatedly changed with the D-spacing to be lower at the overlap region and higher at the gap region. From the results shown in Figures 5 and 6, we can conclude that the piezoelectricity at the gap region is much (about twofolds) higher than that of the overlap region without any ambiguity originating from variations of structure and mechanical properties that is a conventional PFM typically suffers from. The gap region of collagen has randomly kinked networks missing one molecule, while the overlap region consists of five collagen molecules providing a uniform structure. We consider that this randomly kinked networks in the gap region would be more susceptible to the electrical or mechanical perturbation and result in a higher piezoelectric response.

Considering the piezoelectricity to be determined by the molecular structure of an element, it is not surprising that the piezoelectric profile along the collagen fibril has a periodic pattern coordinated to the fibril's periodic surface profile.³⁰ Still, the fact that the gap zone has a much higher value of piezoelectric coefficient than the overlap zone can reinforce the hypothesis that collagen piezoelectricity is one of mechanisms mediating bone mineralization. It is because the piezoelectric profile perfectly matches with the heterogeneous pattern of mechanical property along a mineralized collagen fibril. 19 A pure, unmineralized collagen has lower stiffness on the gap region because of lower packing density of collagen molecules, missing one molecule and a kinked network.5 Once it is mineralized, however, the gap region has higher stiffness because of the stronger reinforcement by mineral as amorphous calcium phosphate (ACP) infiltrates into the intrafibrillar space through the gap region and is then crystallized into mineral nanoplatelets. 59-63 To understand the mechanism of this intrafibrillar mineralization, elucidating the driving force for the ACP infiltration should be the first step.

In previous works, noncollagenous proteins (NCPs), electrostatic interactions, and osmotic pressure have been suggested as a driving force responsible for the ACP infiltration into the intrafibrillar space of collagen. 64-66 Even though each of these mechanisms may explain the ACP infiltration in part, they have limitations to fully delineate it. For instance, even though highlyacidic NCPs had been long believed to direct the nucleation of ACP near the gap zone, 67-70 the underlying procedure was somewhat questionable because their molecule size larger than 40 kDa make them difficult to access to a small intrafibrillar space.^{20,66,71} In a more recent study, it was directly observed by combining cryo-transmission electron microscopy and tomography that the negatively charged ACP complex infiltrates into a fibril through a positively charged A-band region even in the presence of mineral nucleation inhibitors. 60,64 Since then, the electrostatic interaction has been accepted as a prevailing paradigm, 72-74 but it cannot be a sole driving force because it only covers a short-range interaction. ⁶⁶ Specifically, a later study confirmed that there was no difference in the permeability of mineral clusters when cationic and anionic collagen models were examined for intrafibrillar mineralization.⁶⁶ Here, the authors

suggested the osmotic pressure as a long-ranged driving force to supplement the short-ranged electrostatic interaction, as the molecular dynamics simulation showed that the mineral ions with water molecules were transported through the loosely bound gap regions because of the osmotic pressure. ⁶⁶ However, the osmotic pressure depends on a difference of molecular concentrations between intra- and extrafibrillar compartments, and thus, it does not allow room for involving mechanical loading inputs to mediate bone mineralization.

In this regard, the piezoelectricity is a compelling mechanism that can explain both bone's adaptivity to loading and the ACP infiltration into the gap zone as a complementary driving force that can cover the short- and long-range interactions. The piezoelectric property of collagen enables a direct response to loadings by increasing zeta potentials near the collagen surface.⁷⁵ Within a short range, the higher piezoelectricity at the gap zone may supplement the electrostatic interaction to locally modulate the surface potential of a collagen fibril to infiltrate the ACP complex through the gap zone. Furthermore, since the electroosmosis is influenced by the zeta potential, ⁷⁶ the increased zeta potential due to the piezoelectric effect can cause an increase of the electro-osmosis and finally result in an increase of hydraulic permeability at the gap zone. Most importantly, the anisotropic characteristic of collagen piezoelectricity can explain bone's complex response to various types of loadings, such as axial compression, bending, twisting, and shear, developing wellorganized architectures to resist those loadings optimally.

In addition, the piezoresponse of collagen from other tissues that have a different function makes our claim more plausible. For instance, recently, the piezoelectricity of collagen from porcine artery was investigated by the SE-PFM technique. This study showed an opposite trend of piezoelectricity, indicating lower piezoelectricity in gap regions and higher piezoelectricity in overlap regions. This discrepancy of the piezoresponse trend is very interesting because considering the function of this tissue that helps blood flow by maintaining the tissue soft, this tissue must not be mineralized. Therefore, it may indicate that there would be a mechanism to keep the piezoelectricity in the gap region low to prevent tissues from being mineralized by inhibiting the infiltration of mineral clusters. Consequently, this piezoresponse trend of porcine artery collagen also supports the claim that the piezoelectricity of collagen would modulate the mineralization of the tissue.

3. CONCLUSIONS

PFM is a readily approachable technique as a commercially available tool and has been widely applied to various biomaterials. While its setup based on AFM is fairly straightforward, the operation and interpretation still require a great deal of caution especially for quantitative measurement. In this regard, this study was devoted to setting up the protocol for quantitative PFM on biomaterials with anisotropic and heterogenous properties by nature. It is shown that resonanceenhanced PFM is a practical option for biomaterials because it can avoid common vulnerabilities to large mechanical and electrical stimuli while still quantifying the piezoelectric coefficient accurately. Resonance-enhanced PFM in conjunction with DART-PFM enables differentiation of the piezoelectric coefficients between the gap and overlap zones within a single collagen fibril. The protocol developed in this study is applicable to not only collagen but all other types of biomaterials with piezoelectricity. The ability to quantify piezoelectricity of biomaterials with high accuracy will be greatly useful not only in

elucidating its physiological function in various biological processes but also in diagnosing their abnormal activities.

Unravelling the mechanism of bone mineralization is important for addressing the associated clinical issues and suggesting new insights to develop bone-inspired synthetic materials. Even though this study does not demonstrate the direct relationship between the collagen piezoelectricity and interfibrillar mineralization, the PFM results reinforced the possibility of the collagen piezoelectricity as a local modulator mediating the ACP infiltration. To further examine the role of collagen piezoelectricity in bone mineralization, more studies should be followed. As a direct observation, examining the extent of intrafibrillar mineralization on a collagen fibril subject to a controlled mechanical loading is potentially proposed, even though applying a force to a collagen fibril seems to be quite challenging. As an indirect method, a structurally modified collagen may be used to compare the piezoelectric profile and mineralized pattern to corroborate the hypothesis.

4. MATERIALS AND METHODS

4.1. Sample Preparation. Type I collagen extracted from bovine Achilles tendon (Sigma-Aldrich) was used in this study. The collagen powder was dissolved in 0.01 M sulfidic acid at 4 °C overnight to liquify it. Then, the collagen aggregates in sulfidic acid were blended using a commercial blender (Type 4185, Braun) for 10 min at a temperature lower than 4 °C to prevent self-assembly. Phosphate-buffered saline was added to the blended solution to reach a final collagen concentration of 4 μ g/ml. Bare and gold-coated glass substrates were prepared by cleaning with 70% of ethanol and sonicating for 30 s in deionized (DI) water. After the cleaning procedure, they were immersed in the blended collagen solution for 1 h at room temperature so that collagen fibrils were assembled on the surface. Finally, the substrates were taken out and rinsed carefully with DI water before characterization.

4.2. Calibration of Cantilever. To quantitatively evaluate the piezoelectric coefficient of a collagen fibril from the measured PFM amplitude, the AFM cantilever was carefully calibrated in both vertical (out-of-plane) and lateral (in-plane) directions through optical lever sensitivity (OLS).⁷⁷ The OLS (V/nm) is a ratio of a voltage from a photosensitive detector caused by a cantilever deflection per actual cantilever movement toward a hard surface (e.g., a sapphire) captured by an embedded position sensor. While the inverse of OLS for the vertical PFM (VinvOLS, nm/V) was obtained from a force curve of a cantilever on a sapphire surface directly (cf. Figure 7a), the inverse of OLS for lateral PFM (LinvOLS, nm/V) was calculated by considering the cantilever geometry and VinvOLS. 43 The ratio R between the inplane and out-of-plane optical lever amplification corresponds to 2L/ 3h, where L and h indicate the length and height of the cantilever, respectively. 44 Here, the VinvOLS was obtained as 174.02 nm/V and R was 22.22 based on the probe geometry of $L = 500 \,\mu\text{m}$ and $h = 14 \,\mu\text{m}$. Thus, the LinvOLS was determined to be 7.91 nm/V.

After examining the OLS of the cantilever, the Q factor should be investigated to obtain the quantitative piezoresponse (δ) of collagen fibrils from the resonance-enhanced PFM amplitude. This is because the PFM amplitude was amplified by the Q factor at the resonance frequency (i.e., $A_{\rm resonance} = Q\delta$), so the measured PFM amplitude should be divided by Q to obtain the actual piezoelectric strain (δ) . By using the Levenberg–Marquardt algorithm, 51 the experimentally obtained contact resonance curves were fitted to eq 2 (cf. Figure 7b) and their values were estimated to be in the range of 40–110. Finally, eqs 4 and 5 were used to obtain the calibrated piezoresponse of the fibril in the vertical and lateral directions, respectively.

$$A_{\text{pm,vertical}} = \frac{A_{\text{mv}}}{Q} \cdot \text{VinvOLS}$$
(4)

$$A_{\text{pm,lateral}} = \frac{A_{\text{mv}}}{Q} \cdot \text{LinvOLS} = \frac{A_{\text{mv}}}{Q} \cdot \frac{\text{VinvOLS} \cdot 3h}{2L}$$
 (5)

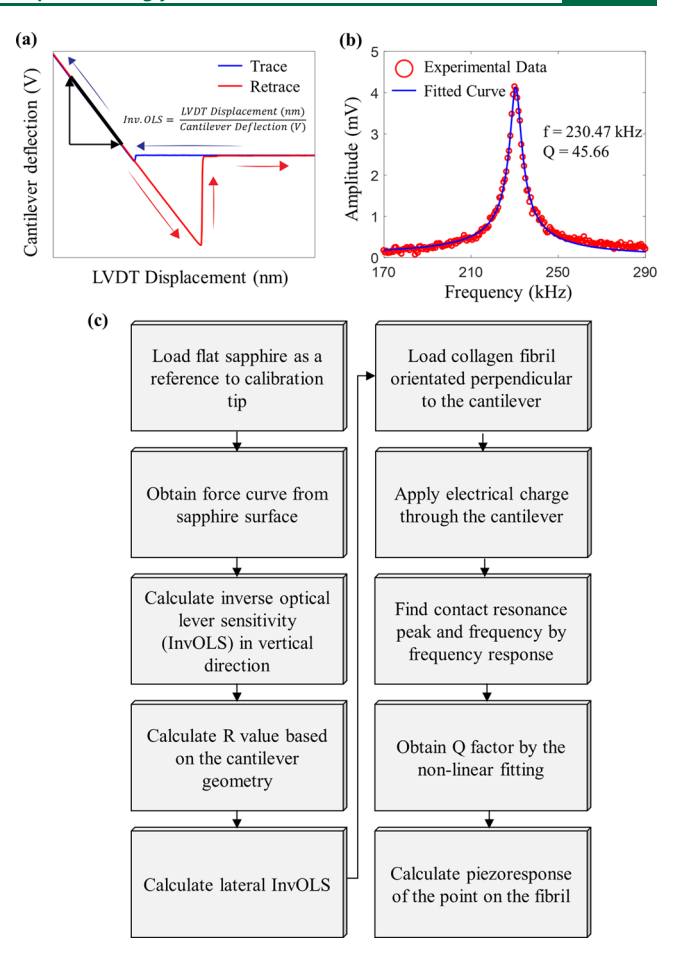


Figure 7. Calibration procedure: (a) a force—displacement curve of a cantilever measured on a sapphire sample to obtain VinvOLS. (b) Contact resonance curve was fitted to eq 2 to obtain the quality factor (Q) for each measurement. (c) Chart summarizing the calibration procedure.

Here, $A_{\rm pm}$ indicates the calibrated piezoresponse amplitude of the collagen fibril, while $A_{\rm mv}$ means the measured PFM signal that is amplified by contact resonance as mentioned in Section 2. The whole calibration process used in this study is summarized in Figure 7c.

4.3. Error Propagation. During the calibration process for lateral PFM, each term involved in the calculation has an error, and the propagation of the error should be carefully considered for the quantitative PFM result. Each term of the PFM result in eqs 4 and 5 was statistically obtained. In order to get the statistical value of VinvOLS, same type cantilevers were randomly selected, and a force curve of the cantilever on a sapphire surface (cf. Figure 7a) was obtained 28 times. As a result, ($\overline{\text{VinvOLS}}$) and $\delta \text{VinvOLS}$ were obtained as 174.02 ± 25.47 pm/mV. Moreover, $A_{\rm mv}$ was measured 10 times depending on each input voltage ranging from 0 to 5 V with a 0.5 V interval through the cantilever body. In total, 110 PFM data points were measured on the collagen fibril surface. Each A_{mv} was determined by the peak value of the frequency response curve, and the Q factor was calculated from each curve, as shown in Figure S1b. In addition, the cantilever specification (3XC-GG, OPUS) was considered statistically. The cantilever's nominal height (\overline{h}) and length (\overline{L}) are 14 and 500 μ m, respectively, with the height range varied from 12 to 16 μ m and the length range varied from 490 to 510 μ m. We assumed that the range of the cantilever geometry (i.e., h and L) indicates 95% of the confidential interval; the standard deviation of δh and δL values would be around 1.02 and 5.10 μ m. Based on this information, the average of $A_{\rm pm}$ was calculated by eq 6

$$\overline{A_{\rm pm}} = \frac{\overline{A_{\rm mv}}}{Q} \cdot \frac{\overline{\text{VinvOLS}} \cdot 3\overline{h}}{2\overline{L}}$$
 (6)

The bar on each term means its average value. The error propagation equation was demonstrated by eq $7\,$

$$\delta A_{\rm pm}^{2} = \left(\frac{\partial A_{\rm pm}}{\partial A_{\rm mv}}\right)^{2} \cdot \delta A_{\rm mv}^{2} + \left(\frac{\partial A_{\rm pm}}{\partial {\rm VinvOLS}}\right)^{2} \cdot \delta {\rm VinvOLS}^{2} + \left(\frac{\partial A_{\rm pm}}{\partial h}\right)^{2} \cdot \delta h^{2} + \left(\frac{\partial A_{\rm pm}}{\partial L}\right)^{2} \cdot \delta L^{2}$$

$$(7)$$

where $\delta A_{\rm pm}$, $\delta A_{\rm mv}$, $\delta {\rm VinvOLS}$, δh , and δL denote the standard deviation of each value, respectively. Finally, $\delta A_{\rm pm}$ can be described as

$$\begin{split} \delta A_{\rm pm} &= |\overline{A_{\rm pm}}| \cdot \\ &\sqrt{\left(\frac{\delta A_{\rm mv}}{\overline{A_{\rm mv}}}\right)^2 + \left(\frac{\delta {\rm VinvOLS}}{\overline{{\rm VinvOLS}}}\right)^2 + \left(\frac{\delta h}{\overline{h}}\right)^2 + \left(\frac{\delta L}{\overline{L}}\right)^2} \end{split} \tag{8}$$

Consequently, the resulting piezoresponse amplitude quantified in this study is accurate with $\pm 21\%$ error.

ASSOCIATED CONTENT

50 Supporting Information

The Supporting Information is available free of charge at https://pubs.acs.org/doi/10.1021/acsbiomaterials.0c01314.

Cantilever calibration and dual AC resonance tracking PFM (PDF)

AUTHOR INFORMATION

Corresponding Author

Hanna Cho — Mechanical and Aerospace Engineering, The Ohio State University, Columbus, Ohio 43210, United States;
o orcid.org/0000-0001-6298-0997; Email: cho.867@ osu.edu

Author

Jinha Kwon – Mechanical and Aerospace Engineering, The Ohio State University, Columbus, Ohio 43210, United States

Complete contact information is available at: https://pubs.acs.org/10.1021/acsbiomaterials.0c01314

Author Contributions

All authors have given approval to the final version of the manuscript. The idea was conceived by H.C., and the experiment and data analysis were performed by J.K. under the guidance of H.C. Both authors contribute equally in writing the manuscript.

Notes

The authors declare no competing financial interest.

ACKNOWLEDGMENTS

This work was supported in part by National Science Foundation (NSF-PFI-TT-1827545) and OSU Material Research Seed Grant Program with funding from NSF-DMR-1420451. These supports are gratefully acknowledged. The authors also appreciate the valuable discussion and comment from Dr. Do-Gyoon Kim (College of Dentistry, The Ohio State University).

REFERENCES

- (1) Fukada, E.; Yasuda, I. Piezoelectric Effects in Collagen. *Jpn. J. Appl. Phys.* **1964**, 3, 117.
- (2) Bassett, C. A. L. ELECTRICAL EFFECTS IN BONE. Sci. Am. 1965, 213, 18–25.

- (3) Gjelsvik, A. Bone Remodeling and Piezoelectricity—I. *J. Biomech.* **1973**, *6*, 69–77.
- (4) Gundjian, A. A.; Chen, H. L. Standardization and Interpretation of the Electromechanical Properties of Bone. *IEEE Trans. Biomed. Eng.* **1974**, *BME-21*, 177–182.
- (5) Athenstaedt, H. Pyroelectric and Piezoelectric Properties of Vertebrates. Ann. N. Y. Acad. Sci. 1974, 238, 68-94.
- (6) Kryszewski, M. Fifty Years of Study of the Piezoelectric Properties of Macromolecular Structured Biological Materials. *Acta Phys. Pol., A* **2004**, *105*, 389–408.
- (7) Minary-Jolandan, M.; Yu, M.-F. Nanoscale Characterization of Isolated Individual Type I Collagen Fibrils: Polarization and Piezoelectricity. *Nanotechnology* **2009**, *20*, 085706.
- (8) Denning, D.; Abu-Rub, M. T.; Zeugolis, D. I.; Habelitz, S.; Pandit, A.; Fertala, A.; Rodriguez, B. J. Electromechanical Properties of Dried Tendon and Isoelectrically Focused Collagen Hydrogels. *Acta Biomater.* **2012**, *8*, 3073–3079.
- (9) Zhou, Z.; Qian, D.; Minary-Jolandan, M. Molecular Mechanism of Polarization and Piezoelectric Effect in Super-Twisted Collagen. *ACS Biomater. Sci. Eng.* **2016**, *2*, 929–936.
- (10) Collagen: Structure and Mechanics; Fratzl, P., Ed.; Springer: New York. 2008.
- (11) Berisio, R.; Vitagliano, L.; Mazzarella, L.; Zagari, A. Crystal Structure of a Collagen-like Polypeptide with Repeating Sequence Pro-Hyp-Gly at 1.4 c5 Resolution: Implications for Collagen Hydration. *Biopolymers* **2000**, *56*, 8–13.
- (12) Martin, R. B.; Burr, D. B.; Sharkey, N. A.; Fyhrie, D. P.. Skeletal Tissue Mechanics, 2nd ed.; Springer: New York, 2015.
- (13) Wallace, D. G. The Relative Contribution of Electrostatic Interactions to Stabilization of Collagen Fibrils. *Biopolymers* **1990**, *29*, 1015–1026.
- (14) Wallace, J. M. Applications of Atomic Force Microscopy for the Assessment of Nanoscale Morphological and Mechanical Properties of Bone. *Bone* **2012**, *50*, 420–427.
- (15) Kadler, K. E.; Holmes, D. F.; Trotter, J. A.; Chapman, J. A. Collagen Fibril Formation. *Biochem. J.* **1996**, 316, 1–11.
- (16) Orgel, J. P. R. O.; Miller, A.; Irving, T. C.; Fischetti, R. F.; Hammersley, A. P.; Wess, T. J. The In Situ Supermolecular Structure of Type I Collagen. *Structure* **2001**, *9*, 1061–1069.
- (17) Denning, D.; Kilpatrick, J. I.; Fukada, E.; Zhang, N.; Habelitz, S.; Fertala, A.; Gilchrist, M. D.; Zhang, Y.; Tofail, S. A. M.; Rodriguez, B. J. Piezoelectric Tensor of Collagen Fibrils Determined at the Nanoscale. *ACS Biomater. Sci. Eng.* **2017**, *3*, 929–935.
- (18) Wegst, U. G. K.; Bai, H.; Saiz, E.; Tomsia, A. P.; Ritchie, R. O. Bioinspired Structural Materials. *Nat. Mater.* **2015**, *14*, 23–36.
- (19) Li, T.; Chang, S.-W.; Rodriguez-Florez, N.; Buehler, M. J.; Shefelbine, S.; Dao, M.; Zeng, K. Studies of Chain Substitution Caused Sub-Fibril Level Differences in Stiffness and Ultrastructure of Wildtype and Oim/Oim Collagen Fibers Using Multifrequency-AFM and Molecular Modeling. *Biomaterials* **2016**, *107*, 15–22.
- (20) Stock, S. R. The Mineral-Collagen Interface in Bone. *Calcif. Tissue Int.* **2015**, 97, 262–280.
- (21) TOMOAIA, G.; PASCA, R.-D. On the Collagen Mineralization. A Review. *Clujul Med.* **2015**, *88*, 15–22.
- (22) Wang, Y.; Azaïs, T.; Robin, M.; Vallée, A.; Catania, C.; Legriel, P.; Pehau-Arnaudet, G.; Babonneau, F.; Giraud-Guille, M.-M.; Nassif, N. The Predominant Role of Collagen in the Nucleation, Growth, Structure and Orientation of Bone Apatite. *Nat. Mater.* **2012**, *11*, 724–732
- (23) Kalinin, S. V.; Rodriguez, B. J.; Jesse, S.; Thundat, T.; Gruverman, A. Electromechanical Imaging of Biological Systems with Sub-10nm Resolution. *Appl. Phys. Lett.* **2005**, *87*, 053901.
- (24) Rodriguez, B. J.; Kalinin, S. V.; Shin, J.; Jesse, S.; Grichko, V.; Thundat, T.; Baddorf, A. P.; Gruverman, A. Electromechanical Imaging of Biomaterials by Scanning Probe Microscopy. *J. Struct. Biol.* **2006**, 153, 151–159.
- (25) Minary-Jolandan, M.; Yu, M.-F. Shear Piezoelectricity in Bone at the Nanoscale. *Appl. Phys. Lett.* **2010**, *97*, 153127.

- (26) Kalinin, S. V.; Rodriguez, B. J.; Shin, J.; Jesse, S.; Grichko, V.; Thundat, T.; Baddorf, A. P.; Gruverman, A. Bioelectromechanical Imaging by Scanning Probe Microscopy: Galvani's Experiment at the Nanoscale. *Ultramicroscopy* **2006**, *106*, 334–340.
- (27) Kalinin, S.; Rar, A.; Jesse, S. A Decade of Piezoresponse Force Microscopy: Progress, Challenges, and Opportunities. *IEEE Trans. Ultrason. Ferroelectrics Freq. Contr.* **2006**, 53, 2226–2252.
- (28) Denning, D.; Paukshto, M. V.; Habelitz, S.; Rodriguez, B. J. Piezoelectric Properties of Aligned Collagen Membranes. *J. Biomed. Mater. Res. B Appl. Biomater.* **2014**, *102*, 284–292.
- (29) Kalinin, S. V.; Rodriguez, B. J.; Jesse, S.; Karapetian, E.; Mirman, B.; Eliseev, E. A.; Morozovska, A. N. Nanoscale Electromechanics of Ferroelectric and Biological Systems: A New Dimension in Scanning Probe Microscopy. *Annu. Rev. Mater. Res.* **2007**, *37*, 189–238.
- (30) Bystrov, V. S.; Seyedhosseini, E.; Kopyl, S.; Bdikin, I. K.; Kholkin, A. L. Piezoelectricity and Ferroelectricity in Biomaterials: Molecular Modeling and Piezoresponse Force Microscopy Measurements. *J. Appl. Phys.* **2014**, *116*, 066803.
- (31) Jesse, S.; Baddorf, A. P.; Kalinin, S. V. Dynamic Behaviour in Piezoresponse Force Microscopy. *Nanotechnology* **2006**, *17*, 1615.
- (32) Kim, S.; Seol, D.; Lu, X.; Alexe, M.; Kim, Y. Electrostatic-Free Piezoresponse Force Microscopy. *Sci. Rep.* **2017**, *7*, 41657.
- (33) Eliseev, E. A.; Morozovska, A. N.; Ievlev, A. V.; Balke, N.; Maksymovych, P.; Tselev, A.; Kalinin, S. V. Electrostrictive and Electrostatic Responses in Contact Mode Voltage Modulated Scanning Probe Microscopies. *Appl. Phys. Lett.* **2014**, *104*, 232901.
- (34) Seol, D.; Kim, B.; Kim, Y. Non-Piezoelectric Effects in Piezoresponse Force Microscopy. *Curr. Appl. Phys.* **2017**, *17*, 661–674.
- (35) Vasudevan, R. K.; Balke, N.; Maksymovych, P.; Jesse, S.; Kalinin, S. V. Ferroelectric or Non-Ferroelectric: Why so Many Materials Exhibit "Ferroelectricity" on the Nanoscale. *Appl. Phys. Rev.* **2017**, *4*, 021302.
- (36) Rodriguez, B. J.; Callahan, C.; Kalinin, S. V.; Proksch, R. Dual-Frequency Resonance-Tracking Atomic Force Microscopy. *Nanotechnology* **2007**, *18*, 475504.
- (37) Lozano, J. R.; Garcia, R. Theory of Multifrequency Atomic Force Microscopy. *Phys. Rev. Lett.* **2008**, *100*, 076102.
- (38) Garcia, R.; Herruzo, E. T. The Emergence of Multifrequency Force Microscopy. *Nat. Nanotechnol.* **2012**, *7*, 217–226.
- (39) Santos, S.; Lai, C.-Y.; Olukan, T.; Chiesa, M. Multifrequency AFM: From Origins to Convergence. *Nanoscale* **2017**, *9*, 5038–5043.
- (40) Kalinin, S. V.; Rodriguez, B. J.; Jesse, S.; Shin, J.; Baddorf, A. P.; Gupta, P.; Jain, H.; Williams, D. B.; Gruverman, A. Vector Piezoresponse Force Microscopy. *Microsc. Microanal.* **2006**, *12*, 206–220
- (41) Sharma, P.; Wu, D.; Poddar, S.; Reece, T. J.; Ducharme, S.; Gruverman, A. Orientational Imaging in Polar Polymers by Piezoresponse Force Microscopy. *J. Appl. Phys.* **2011**, *110*, 052010.
- (42) Dharmasena, S. M.; Yang, Z.; Kim, S.; Bergman, L. A.; Vakakis, A. F.; Cho, H. Ultimate Decoupling between Surface Topography and Material Functionality in Atomic Force Microscopy Using an Inner-Paddled Cantilever. ACS Nano 2018, 12, 5559–5569.
- (43) Peter, F.; Rüdiger, A.; Waser, R.; Szot, K.; Reichenberg, B. Comparison of In-Plane and out-of-Plane Optical Amplification in AFM Measurements. *Rev. Sci. Instrum.* **2005**, *76*, 046101.
- (44) Peter, F.; Rudiger, A.; Szot, K.; Waser, R.; Reichenberg, B. Sample-Tip Interaction of Piezoresponse Force Microscopy in Ferroelectric Nanostructures. *IEEE Trans. Ultrason. Ferroelectrics Freq. Contr.* **2006**, *53*, 2253–2260.
- (45) Choi, H.; Hong, S.; No, K. Quantitative Measurement of In-Plane Cantilever Torsion for Calibrating Lateral Piezoresponse Force Microscopy. *Rev. Sci. Instrum.* **2011**, 82, 113706.
- (46) Minary-Jolandan, M.; Yu, M.-F. Uncovering Nanoscale Electromechanical Heterogeneity in the Subfibrillar Structure of Collagen Fibrils Responsible for the Piezoelectricity of Bone. *ACS Nano* **2009**, *3*, 1859–1863.
- (47) de Jong, M.; Chen, W.; Geerlings, H.; Asta, M.; Persson, K. A. A Database to Enable Discovery and Design of Piezoelectric Materials. *Sci. Data* **2015**, *2*, 150053.

- (48) Liu, Y.; Luo, D.; Wang, T. Hierarchical Structures of Bone and Bioinspired Bone Tissue Engineering. *Small* **2016**, *12*, 4611–4632.
- (49) Jesse, S.; Mirman, B.; Kalinin, S. V. Resonance Enhancement in Piezoresponse Force Microscopy: Mapping Electromechanical Activity, Contact Stiffness, and Q Factor. *Appl. Phys. Lett.* **2006**, *89*, 022906.
- (50) García, R.; Pérez, R. Dynamic Atomic Force Microscopy Methods. Surf. Sci. Rep. 2002, 47, 197–301.
- (51) Seber, G. A. F.; Wild, C. J. Computational Methods for Nonlinear Least Squares. In *Nonlinear Regression*; John Wiley & Sons, Ltd, 2005; pp 619–660.
- (52) Nair, M.; Calahorra, Y.; Kar-Narayan, S.; Best, S. M.; Cameron, R. E. Self-Assembly of Collagen Bundles and Enhanced Piezoelectricity Induced by Chemical Crosslinking. *Nanoscale* **2019**, *11*, 15120–15130.
- (53) Yang, S. M.; Mazet, L.; Okatan, M. B.; Jesse, S.; Niu, G.; Schroeder, T.; Schamm-Chardon, S.; Dubourdieu, C.; Baddorf, A. P.; Kalinin, S. V. Decoupling Indirect Topographic Cross-Talk in Band Excitation Piezoresponse Force Microscopy Imaging and Spectroscopy. *Appl. Phys. Lett.* **2016**, *108*, 252902.
- (54) Jesse, S.; Guo, S.; Kumar, A.; Rodriguez, B. J.; Proksch, R.; Kalinin, S. V. Resolution Theory, and Static and Frequency-Dependent Cross-Talk in Piezoresponse Force Microscopy. *Nanotechnology* **2010**, 21, 405703.
- (55) Huang, B.; Esfahani, E. N.; Li, J. Mapping Intrinsic Electromechanical Responses at the Nanoscale via Sequential Excitation Scanning Probe Microscopy Empowered by Deep Data. *Natl. Sci. Rev.* **2019**, *6*, 55–63.
- (56) Liu, Y.; Seidel, J.; Li, J. Multiferroics under the Tip: Probing Magnetoelectric Coupling at the Nanoscale. *Natl. Sci. Rev.* **2019**, *6*, 626–628
- (57) Jiang, P.; Huang, B.; Wei, L.; Yan, F.; Huang, X.; Li, Y.; Xie, S.; Pan, K.; Liu, Y.; Li, J. Resolving Fine Electromechanical Structure of Collagen Fibrils via Sequential Excitation Piezoresponse Force Microscopy. *Nanotechnology* **2019**, *30*, 205703.
- (58) Minary-Jolandan, M.; Yu, M.-F. Nanomechanical Heterogeneity in the Gap and Overlap Regions of Type I Collagen Fibrils with Implications for Bone Heterogeneity. *Biomacromolecules* **2009**, *10*, 2565–2570.
- (59) Nair, A. K.; Gautieri, A.; Chang, S.-W.; Buehler, M. J. Molecular Mechanics of Mineralized Collagen Fibrils in Bone. *Nat. Commun.* **2013**, *4*, 1724.
- (60) Nudelman, F.; Lausch, A. J.; Sommerdijk, N. A. J. M.; Sone, E. D. In Vitro Models of Collagen Biomineralization. *J. Struct. Biol.* **2013**, *183*, 258–269.
- (61) Landis, W. J.; Jacquet, R. Association of Calcium and Phosphate Ions with Collagen in the Mineralization of Vertebrate Tissues. *Calcif. Tissue Int.* **2013**, 93, 329–337.
- (62) Nair, A. K.; Gautieri, A.; Buehler, M. J. Role of Intrafibrillar Collagen Mineralization in Defining the Compressive Properties of Nascent Bone. *Biomacromolecules* **2014**, *15*, 2494–2500.
- (63) Lotsari, A.; Rajasekharan, A. K.; Halvarsson, M.; Andersson, M. Transformation of Amorphous Calcium Phosphate to Bone-like Apatite. *Nat. Commun.* **2018**, *9*, 4170.
- (64) Nudelman, F.; Pieterse, K.; George, A.; Bomans, P. H. H.; Friedrich, H.; Brylka, L. J.; Hilbers, P. A. J.; de With, G.; Sommerdijk, N. A. J. M. The Role of Collagen in Bone Apatite Formation in the Presence of Hydroxyapatite Nucleation Inhibitors. *Nat. Mater.* **2010**, *9*, 1004–1009.
- (65) Boonrungsiman, S.; Gentleman, E.; Carzaniga, R.; Evans, N. D.; McComb, D. W.; Porter, A. E.; Stevens, M. M. The Role of Intracellular Calcium Phosphate in Osteoblast-Mediated Bone Apatite Formation. *Proc. Natl. Acad. Sci.* **2012**, *109*, 14170–14175.
- (66) Niu, L.-n.; Jee, S. E.; Jiao, K.; Tonggu, L.; Li, M.; Wang, L.; Yang, Y.-d.; Bian, J.-h.; Breschi, L.; Jang, S. S.; Chen, J.-h.; Pashley, D. H.; Tay, F. R. Collagen Intrafibrillar Mineralization as a Result of the Balance between Osmotic Equilibrium and Electroneutrality. *Nat. Mater.* **2016**, 16, 370–378.
- (67) Boskey, A. L. Noncollagenous Matrix Proteins and Their Role in Mineralization. *Bone Miner.* **1989**, *6*, 111–123.

- (68) Vetter, U.; Fisher, L. W.; Mintz, K. P.; Kopp, J. B.; Tuross, N.; Termine, J. D.; Robey, P. G. Osteogenesis Imperfecta: Changes in Noncollagenous Proteins in Bone. *J. Bone Miner. Res.* **1991**, *6*, 501–505.
- (69) Roach, H. Why Does Bone Matrix Contain Non-Collagenous Proteins? The Possible Roles of Osteocalcin, Osteonectin, Osteopontin and Bone Sialoprotein in Bone Mineralisation and Resorption. *Cell Biol. Int.* **1994**, *18*, 617–628.
- (70) Gorski, J. P. Biomineralization of Bone: A Fresh View of the Roles of Non-Collagenous Proteins. *Front. Biosci.* **2011**, *16*, 2598–2621.
- (71) Toroian, D.; Lim, J. E.; Price, P. A. The Size Exclusion Characteristics of Type I Collagen IMPLICATIONS FOR THE ROLE OF NONCOLLAGENOUS BONE CONSTITUENTS IN MINERALIZATION. *J. Biol. Chem.* **2007**, 282, 22437—22447.
- (72) Cölfen, H. Crystal-Clear View. Nat. Mater. 2010, 9, 960-961.
- (73) Landis, W. J.; Silver, F. H. Mineral Deposition in the Extracellular Matrices of Vertebrate Tissues: Identification of Possible Apatite Nucleation Sites on Type I Collagen. *Cells Tissues Organs* **2009**, *189*, 20–24
- (74) Silver, F. H.; Landis, W. J. Deposition of Apatite in Mineralizing Vertebrate Extracellular Matrices: A Model of Possible Nucleation Sites on Type I Collagen. *Connect. Tissue Res.* **2011**, *52*, 242–254.
- (75) Ahn, A. C.; Grodzinsky, A. J. Relevance of Collagen Piezoelectricity to "Wolff's Law": A Critical Review. *Med. Eng. Phys.* **2009**, *31*, 733–741.
- (76) Bowen, W. R.; Clark, R. A. Electro-Osmosis at Microporous Membranes and the Determination of Zeta-Potential. *J. Colloid Interface Sci.* **1984**, *97*, 401–409.
- (77) D'Costa, N. P.; Hoh, J. H. Calibration of Optical Lever Sensitivity for Atomic Force Microscopy. *Rev. Sci. Instrum.* **1995**, *66*, 5096–5097.